

STRUT-BRACED WING INDUCED DRAG MODELING FOR REGIONAL TURBOPROP AIRCRAFT DESIGN

Giuseppe Grazioso¹ & Agostino De Marco²

¹PhD Candidate, University of Naples Federico II, Dept. of Industrial Engineering, giuseppe.grazioso@unina.it ²Associate professor, University of Naples Federico II, Dept. of Industrial Engineering, agodemar@unina.it

Abstract

To align with the new environmental goals established by the European Commission in its documents "Flightpath 2050: Europe's Vision for Aviation" and "Fly The Green Deal," aircraft manufacturers, research centers, and universities have collaborated extensively to develop new aircraft concepts and configurations to reduce the environmental impact of aviation. The primary objective is to identify innovative technologies and aircraft configurations that can significantly reduce emissions and fuel consumption. In recent years, the strut-braced wing (SBW) configuration has attracted significant interest from aircraft manufacturers and research centers. This aircraft configuration combines the aerodynamic efficiency benefits of a high aspect ratio wing with a reduction in wing weight compared to a high aspect ratio cantilever wing. The aerodynamic benefit achieved from the SBW configuration lies in the reduction of induced drag. However, two side effects need to be considered. The strut initially causes an increase in parasite drag. Secondly, the reduction in the induced drag term is counteracted by the mutual interference between the wing and the strut. For these reasons, a parametric investigation was conducted on a regional turboprop aircraft to better understand and quantify the increase in induced drag caused by wing-strut interference. Various geometric design variables were taken into account during an aerodynamic investigation conducted using the commercial panel method solver FlightStream®. The achieved results have been used to develop a response surface to estimate this aerodynamic effect. Finally, this numerical model is applied to the preliminary design of a strut-braced wing version of the ATR72-600 aircraft to assess the influence of the developed model on block fuel reduction.

Keywords: Strut-Braced-Wing, Aerodynamic parametric modelling, Aerodynamic design, Aircraft design

1. Introduction

In Europe, the aviation sector contributes approximately 3% of total greenhouse gas emissions. According to projections from Airbus and Boeing, passenger-kilometers are expected to increase by 5% annually over the next two decades [1]. Therefore, it is crucial to address the increase in pollution alongside the growing demand for air travel. To mitigate the environmental impact, the European community introduced "Flightpath 2050: Europe's Vision for Aviation" in 2011, outlining the goals and challenges for the aviation industry to achieve by 2050 [2] This initiative was revised in 2022 with an updated version called "Fly the Green Deal"[3]. The initial goals set by ACARE in Flightpath 2050 have been revised in "Fly the Green Deal," focusing on three different time segments: 2030, 2035, and 2050. The goals for the regional aviation segment are summarized as follows:

- By 2030, net CO2 emissions from all intra-EU flights and those departing the EU will be reduced by 55% compared to a 1990 baseline. Additionally, non-CO2 climate effects will be fully understood, managed, monitored, and reduction targets will be set in line with the latest scientific understanding and mitigation solutions
- By 2035, new technologies, fuels, and operational procedures will result in a 30% reduction of non-CO2 climate effects for all intra-EU flights and those departing the EU relative to a 1990 baseline.

 By 2050, net-zero CO2 emissions will be achieved for all intra-EU flights and those departing the EU. Furthermore, new technologies and operational procedures will result in a 90% reduction in NOx, non-volatile particulate matter, and warming contrail cirrus from all intra-EU flights and those departing the EU relative to the year 2000.

To align with the ACARE goals, various solutions have been explored in recent years, from unconventional tailplane designs [4, 5], coming to DEP systems [6] arriving to new wing high-lift systems developing[7]. Among the proposed solutions, a promising aircraft architecture that does not require a complete redesign of the propulsion system, as is necessary for hybrid electric architectures [8, 9, 10, 11], is the use of ultra-high aspect ratio wings (UHARW). Recent research has high-lighted the potential advantages of this setup, particularly in achieving a significant decrease in fuel consumption by improving lift-to-drag ratios and minimizing induced drag factors. However, designing wings with extremely high aspect ratios presents challenges. These include increased bending moments at the wing root, necessitating thicker wings for enhanced stiffness, and higher wingtip deflection due to increased elasticity. Researchers have investigated different architectural solutions to address these challenges, such as strut-braced wings (SBW), multi-fuselage designs[12], and folding wings. These approaches aim to balance the aerodynamic advantages of UHARW with the structural considerations essential for safe and efficient aircraft design.

The Strut-Braced Wing (SBW) concept is a specific configuration within the broader Truss-Braced Wing (TBW) design, comprising various components: the wing, primary wing struts, jury struts, and a truss support structure attached to the fuselage. The primary wing struts and jury struts serve distinct purposes, see Figure 1. Primary wing struts are designed to absorb wing bending loads and transfer them to the lower fuselage carry-through or alter the load direction. Jury struts shift buckling modes to higher frequencies, thereby stabilizing the wing and/or primary wing struts. When the truss-braced wing includes only a single primary wing strut, this configuration is termed a strut-braced wing [13].

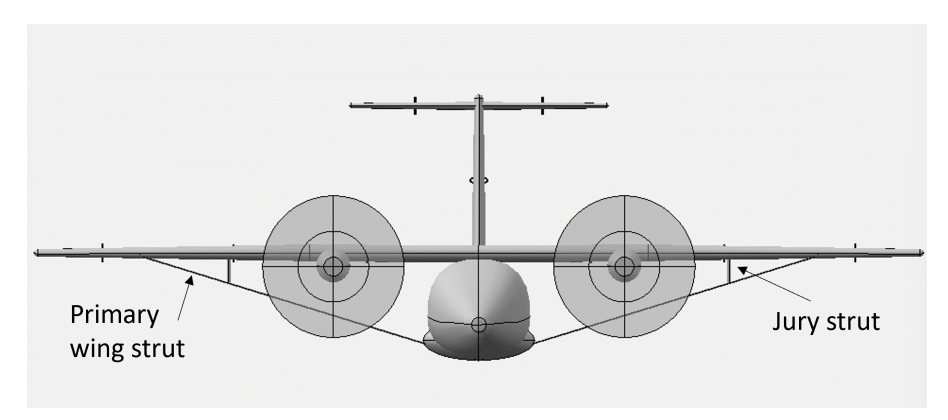


Figure 1 – Truss braced wing geometry showing strut definitions.

From a structural design perspective, the addition of a strut enables the creation of a lighter, high-aspect-ratio wing. The primary wing strut reduces the bending moment at the wing root chord by supporting a portion of the wing bending moment and transferring it to the fuselage carry-through structure as axial load. This reduction in the wing bending moment at the root chord, which increases with the strut chord, compared to the wing bending moment in a cantilever wing configuration, allows for the design of a thinner wing box. Consequently, a thinner wing box results in reduced airfoil parasite drag. An example of a possible wing bending moment diagram for SBW and cantilever wing configurations is shown in Figure 2. The reduction in wing weight is particularly advantageous for high-aspect-ratio wing configurations, although careful consideration must be given to the choice of strut chord value. When considering the total aircraft drag estimation using the parabolic drag polar formulation

$$C_D = C_{D_0} + \frac{C_L^2}{\pi \, \mathcal{R} \, e} \tag{1}$$

two effects contribute to the reduction of the induced drag term: (i) the lower wing weight, leading to a lower aircraft weight and hence a lower lift coefficient value, and (ii) the high aspect ratio value.

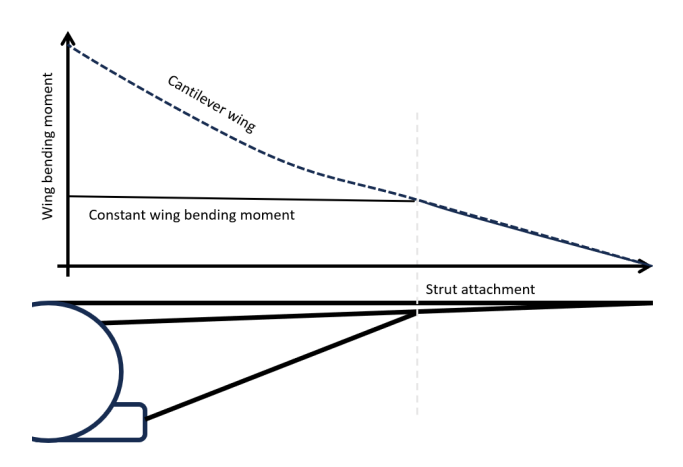


Figure 2 – SBW vs. cantilever bending moment spanwise distribution.

While the SBW configuration offers benefits, it also presents certain drawbacks. Firstly, the presence of the wing strut increases the zero-lift drag coefficient, especially when the strut chord length is not sufficiently short. Secondly, if the strut is treated as a lifting body, the pressure distribution along the strut interacts with that along the wing. This interaction alters the load distribution along the wing, deviating further from the ideal elliptical load distribution. As a result, the Oswald efficiency factor decreases, leading to increased induced drag. Figure 3 illustrates a comparison of the wingspan loading, expressed as $c(y) \cdot cl(y)$, calculated for the cantilever, SBW, and the equivalent elliptical wing version of the same wing planform. Additionally, the load distribution for the SBW configuration is subdivided into the load along the wing and the load along the strut to illustrate the change in the wing loading shape for the SBW concept. The pressure distribution generated by the strut causes the wing's load shape to change from the curve represented in blue (cantilever wing loading) to the curve in purple (SBW wing loading).

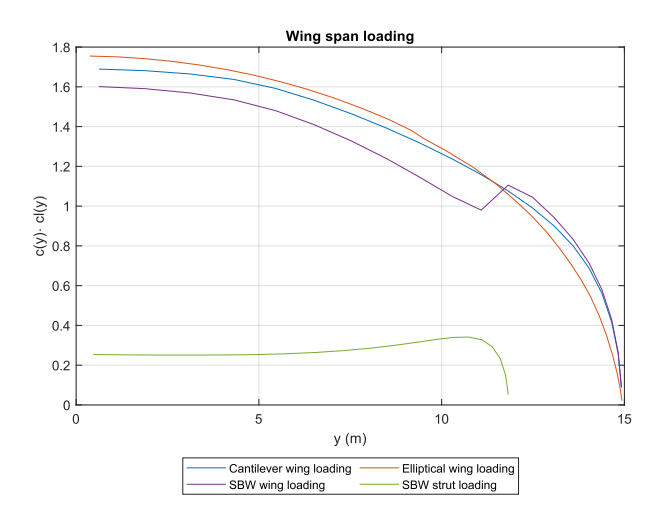


Figure 3 – Wing span loading expressed as $c(y) \cdot cl(y)$ comparison among SBW, two-panel wing and the equivalent elliptical wing version of the same wing planform.

Therefore, while the SBW configuration offers advantages in reducing the $C_{\rm D}$ induced term, the actual change in drag may not meet the expected value. Consequently, this study focuses on a parameter that has not been extensively investigated: the wing-strut interference effect. The objective is to quantify the reduction in Oswald's factor that the SBW configuration may experience compared to the cantilever wing configuration if the wing-strut mutual interaction is not correctly optimized. Once the wing-strut mutual interaction is investigated, the impact of this developed model will be assessed at the aircraft level, focusing on the design of a strut-braced wing version of the ATR72 aircraft.

2. Methodologies and Assumptions

2.1 Software used

To assess the reduction in Oswald's factor produced by the SBW configuration compared to the cantilever version of the same wing planform, an aerodynamic investigation was conducted using FlightStream® as the aerodynamic solver. FlightStream® is a surface vorticity flow solver designed to assist users in developing optimized designs for compressible and incompressible subsonic and transonic vehicles [14]. This solver uses surface vorticity on an unstructured surface mesh to predict loads with attached flow [15, 16]. It employs the Fast Multipole Method to handle the merging of farfield potential inviscid source/doublet bodies into a single body, thereby evaluating the overall impact on a single near-field body [15]. FlightStream® also has the capability to model the aerodynamic field and characterize the boundary layer for laminar, turbulent, and transitional regimes [15].

To conduct this aerodynamic investigation, an automatic workflow was established. The wing geometry was designed using a typical wing planform employed for regional turboprop applications. This geometry was then analyzed using the selected aerodynamic solver, and the obtained aerodynamic results were post-processed to extract the reduction in Oswald's factor. The workflow was developed in Matlab® and is depicted in Figure 4. Figure 5) represents an example of the assumed wing planform. The wing geometry was modeled using the JPAD Modeller software [17]. This software models each lifting surface planform through a series of panels, each characterized by various geometric features such as root chord, tip chord, span, sweep, and dihedral angle. An example of a two-panel wing planform is shown in Figure 6.

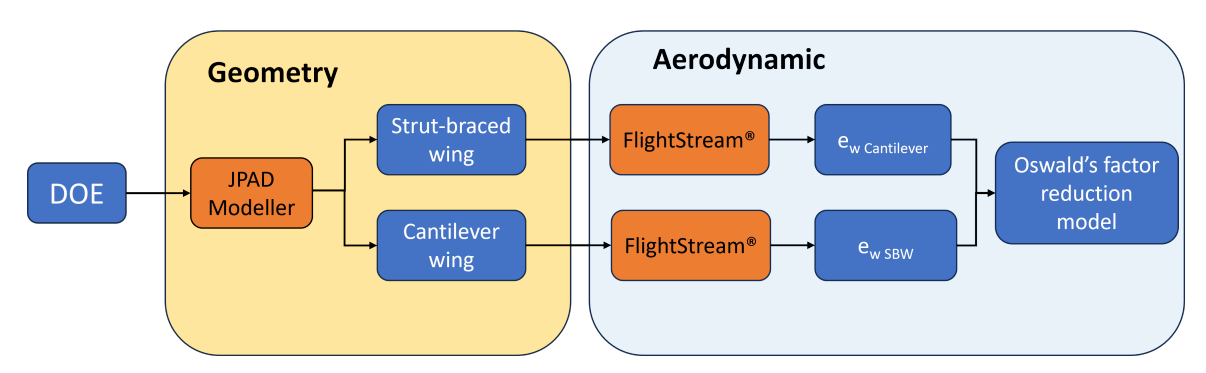


Figure 4 – Analysis workflow schema.

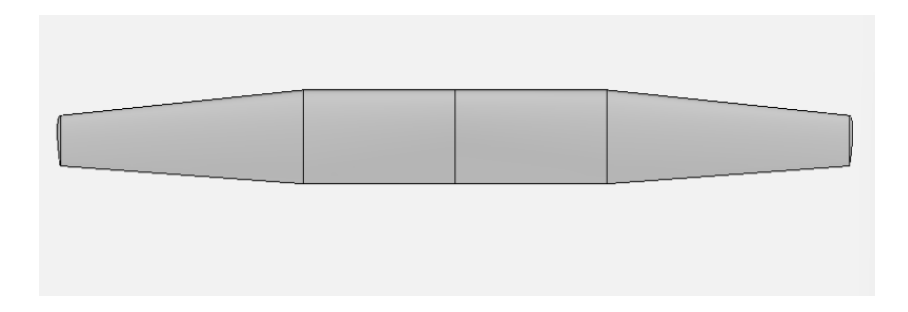


Figure 5 – Typical wing planform for regional turboprop applications assumed in the aerodynamic investigation.

The JPAD Modeller software is the first standalone product of the JPAD software family. It was developed at the University of Naples Federico II by the DAF Research group and is commercialized by SmartUp Engineering s.r.l., an academic spin-off company of the University of Naples Federico II [18, 19, 20]. With a simple user interface (UI), JPAD Modeller allows users to generate and manage parametrically defined aircraft and their CAD models. Each primary aircraft component, such as lifting surfaces, fuselage, cabin, engines, and movable parts, can be customized according to a preselected set of input parameters. This approach is designed to offer sufficient flexibility while minimizing the number of input variables.

JPAD Modeller also allows for easy export of the aircraft CAD and parametric models in several

file formats, including CPACS, OpenVSP, and FlightStream®. The connection to the FlightStream® software is established via the FlightStream® Component Cross Section (CCS) file format [21]. Using this link, the JPAD Modeller user can export and analyze the aerodynamic characteristics of their aircraft efficiently. Thanks to the existing link between JPAD Modeller and FlightStream®, JPAD was chosen as the parametric geometry generator in the designed workflow.

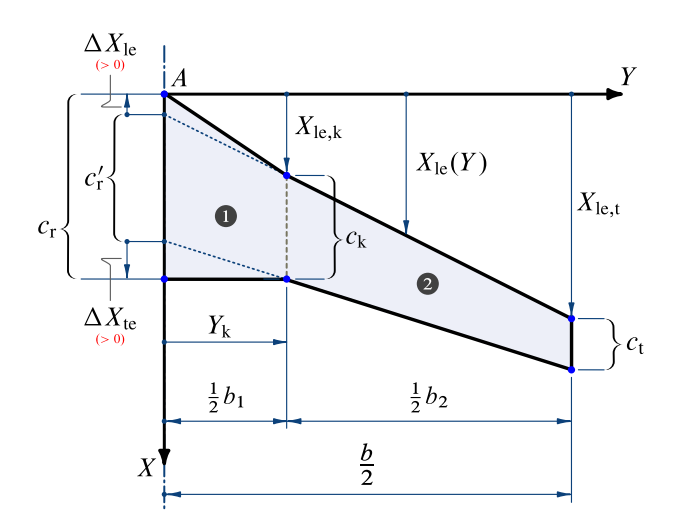


Figure 6 – Wing planform definition of two-panel wing used by JPAD software.

2.2 Cantilever and SBW design methodology

Six design geometric variables were assumed and used to build a generic wing planform from which the cantilever wing geometry and the SBW configuration were derived. All the selected variables combined in a full factorial design, have been selected as design parameters to understand their impact on the aerodynamic module. The design variables are listed in Table 1. , which includes the selected boundary values and the number of levels assumed for each design variable considered in constructing the full factorial design plane. Four variables are associated with the cantilever wing configuration, while the other two are related to the SBW. The variables related to the cantilever solution are wing area (S_W) , wing aspect ratio (AR), wing taper ratio (λ) , and wing thickness ratio sets (t_c) . The parameters related to the SBW configuration are the wing-strut intersection as a fraction of the wing semi-span (η_s) and the ratio between the strut chord and the wing chord at the wing-strut intersection, known as the strut chord ratio (c_s/c) .

Table 1 – Geom			
			l aerodynamic investigation.

Full factorial design variables						
Variable	Description	Min. value	Max. value	Levels		
S_W	wing area	50 m ²	100m^2	4		
R	wing aspect ratio	10	20	4		
λ	wing taper ratio	0.4	0.8	4		
t_{c}	wing thickness ratio sets	Case-1	Case-4	4		
$oldsymbol{\eta}_s$	strut attachment semi-spanwise position	0.35	0.8	3		
c_s/c	strut chord ratio	0.2	0.6	3		

2.2.1 Cantilever wing geometry model

The cantilever wing planform is designed based on the following two assumptions:

• The wing is a two-panel wing where the first wing panel is rectangular while the second is trapezoidal.

• the span of the rectangular wing panel has been assumed to be the 66% of the total wing span, $\eta_{\rm rect}=0.66$.

From these assumptions, the following formula derives the value of the wing root chord as a function of the taper ratio (λ) , wing surface area (S_W) , and wing aspect ratio (AR):

$$c_{root} = \frac{2\sqrt{S}}{\sqrt{AR} \left[1 + \lambda + \frac{1}{2} \eta_{\text{rect}} (1 - \lambda) \right]}$$
 (2)

To complete the design of the cantilever wing geometry model, the wing airfoils must be chosen. The selected airfoils are from the NACA 5-series, specifically of the type 230XX. Four different combinations for root, kink, and tip section thickness ratios have been selected. All t_c sets are provided in Table 2.

Spanwise NACA 5 series airfoil selection list					
t_c sets \mid wing root section \mid wing kink section \mid wing tip section					
Case-1	23018	23018	23015		
Case-2	23016	23016	23013		
Case-3	23020	23020	23017		
Case-4	23015	23015	23010		

Table 2 – Airfoil thickness ratio values selected for root, kink and wing section.

2.2.2 Strut Braced Wing (SBW) geometry model

The SBW wing geometry is derived from the cantilever wing configuration by incorporating a primary wing strut. The primary strut was modeled based on the following assumptions:

- The z-coordinate of the strut's leading edge at the strut-fuselage intersection is set to 25% of the fuselage section height, measured from the bottom of the fuselage section (Figure 7).
- The x-coordinate of the strut's leading edge at the wing-strut intersection is set at 20% of the wing chord at the attachment point, measured from the wing's leading edge. If this requirement could not be met for a specific combination of design variables, an iterative procedure was developed to identify a new starting point that minimizes the distance from the original point.
- the strut is modeled as a straight lifting surface with a constant chord.
- the airfoil chosen for each strut section is NACA0012.

These assumptions with the selected value for the design variables c_s/c and η_s allows JPAD Modeller to create the SBW geometry model.

2.3 Aerodynamic analysis

The aerodynamic characteristics of the two wing geometries were analyzed using the same solver settings, as reported in Table 3.

To validate the accuracy of the FlightStream® software, a random value was selected for each design parameter within the assigned boundaries, as shown in Table 4. Using these geometry design parameters, the corresponding SBW geometry model was created and analyzed using both FlightStream® and Simcenter STAR-CCM+, a commercial CFD solver [22]. Figure 8 depicts the geometry model analyzed in STAR-CCM+. Figures 9 and 10 present the comparison of results between STAR-CCM+ and FlightStream® for the analyzed geometry. In Figure 9 the lift curves are compared, showing that in the linear region, the results are very similar, with a slight difference in the slope of the lift coefficient curve, where FlightStream® yields a slightly higher value compared to the RANS analysis results. Given that the region under investigation is the linear region, the analysis results obtained

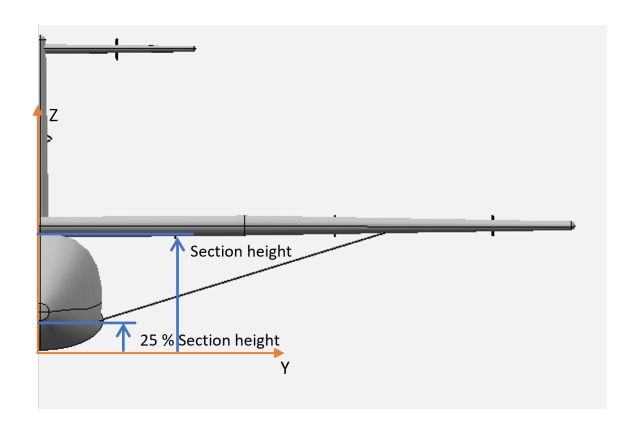


Figure 7 – Z-coordinate for the strut's leading edge at strut-fuselage intersection.

with FlightStream® are considered acceptable. Figure 10 compares the distribution of the lift coefficient along the wingspan and the strut semi-span. The results achieved with FlightStream® closely match those obtained using STAR-CCM+. This figure highlights that the strut alters the distribution of the lift coefficient, increasing its deviation from the ideal elliptical $c_l(y)$ distribution, which corresponds to the minimum induced drag value (Oswald factor unity). This underscores the utility of a solver that can produce results comparable to CFD analysis but with significantly reduced computational costs, facilitating the estimation of the effect of design variables on the wing strut's aerodynamic impact, which affects the spanwise distribution of the lift coefficient.

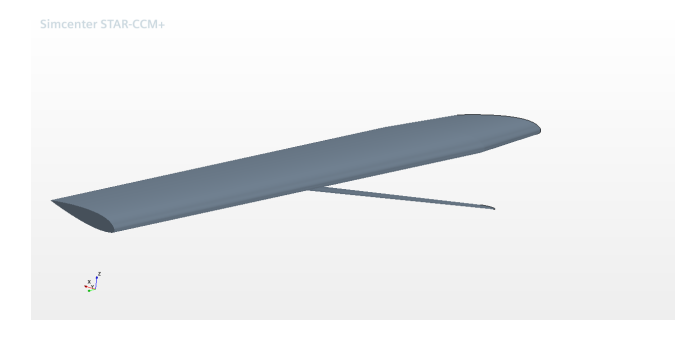


Figure 8 – Geometric representation for the validation test case in Simcenter STAR-CCM+

A total of 2,304 SBW geometry models were generated for analysis using the developed workflow, as depicted in Figure4. To represent the design space for the cantilever wing geometry model, 256 cases were generated. Each case represents a combination of design variables used by the JPAD Modeller software to generate geometric models for both the cantilever and strut-braced configurations. These geometries were analyzed using FlightStream® under the same operating conditions defined in Table 3. The aerodynamic results for the two wing configurations were post-processed to extract Oswald's factors, which were then interpolated using the radial basis functions (RBF) technique to create two distinct surrogate RBF models, one for each wing configuration. These models were compared to quantify the variation in Oswald's efficiency factor introduced by the strut-braced wing compared to the cantilever wing version.

An example of the results provided by this model is illustrated in Figure 11. This figure shows the comparison between the strut-braced version of the ATR-72 wing ($S_w = 61 \, \mathrm{m}^2$, $\mathcal{R} = 12$, $\lambda = 0.5639$, t_c -set = Case-1) and the cantilever version. The results are presented using a contour plot, illustrating the influence of the two SBW geometry parameters. From this contour plot, by selecting specific values for η_s and c_s/c , it is possible to estimate the reduction in Oswald's efficiency factor. This factor is expressed as a percentage and can be applied to the Oswald factor estimated for the cantilever wing version [23]. The figure demonstrates that as η_s and the ratio of strut chord to wing chord (c_s/c) increase, the reduction in Oswald's factor also increases. This is attributed to the larger strut chord and a more outward position of the attachment towards the wing tip, both of which significantly impact wing loading, increasing the deviation from the ideal elliptical wing loading.

Table 3 – Aerodynamic settings for the aerodynamic analysis in FlightStream®

FlightStream® aerodynamic analysis settings				
Fluid properties				
Altitude	20 000 ft			
Density	$0.6526\mathrm{kg/m^3}$			
Pressure	46.563 Pa			
Speed of sound	$316.032 \mathrm{m/s}$			
Temperature	248.526 K			
Dynamic viscosity	0.000016 Pa/s			
Solver se	ettings			
Solver type	steady			
Boundary layer type	Transitional Turbulent			
Viscous coupling	enable			
Flow separation	enable			
Iteration number	800			
Convergence limit	0.00005			
Processors	36			
Symmetry type	Plane			
symmetry periodicity	1			
Angle of attack min	$-2 \deg$			
Angle of attack max	4 deg			
Angle of attack delta	1 deg			
Free stream velocity	138.9 m/s			
Free stream ref. velocity	138.9 m/s			
Side slip angle min	0 deg			
Side slip angle max	0 deg			
Side slip angle delta	0 deg			

Using the results obtained by the developed aerodynamic model is possible to estimate the parabolic drag polar for the SBW configuration using the equations (3), (4), and (5).

$$C_{D,\text{SBW}} = C_{D0,\text{Aircraft}} + C_{D0,\text{Strut}} + \frac{1}{\pi \cdot AR \cdot e_{\text{SBW}}} \cdot CL^2$$
(3)

$$e_{\text{SBW}} = e_{\text{cantilever}} \cdot (1 - k_{\text{red}})$$
 (4)

$$k_{\text{red}} = \mathscr{F}_{\text{red}}(S_w, AR, \lambda, tc\text{-set}, \eta_s, c_s/c)$$
(5)

where \mathscr{F}_{red} is the developed wing Oswald factor reduction model.

2.4 Wing weight estimation method

The the results achieved using the developed aerodynamic model becomes particularly interesting when is coupled with a wing weight estimation method, in such a way is possible to evaluate the impact of the developed aerodynamic model at aircraft level at the preliminary design phase.

The wing weight estimation method selected in this work that is the one developed by G. Chiozzotto [24], which is based on a physics-based wing weight estimation methodology, where particular importance is given to the aeroelastic effects caused by the high flexibility of the high aspect ratio wings. This methodology allows for estimating the wing mass for both cantilever and SBW configurations. This methodology allows for estimating the wing mass for both cantilever and SBW configurations. Equation (6) defines the method for evaluating the wing mass:

$$m_w = k_{ail} \cdot (m_{covers} + m_{webs+ribs}) + m_{sec} + m_{strut}$$
(6)

Table 4 – Geometry characteristic for the FlightStream® test case validation against CFD solver STAR-CCM+.

Geometry characteristics of the validation test case			
Design variable	Symbol	Value	
Wing surface	S_W	$73.87 \mathrm{m}^2$	
Aspect ratio	Æ	12.083	
Wing thickness ratio set	t_c -set	Case-1	
Wing taper ratio	λ	0.485	
Strut chord ratio	c_s/c	0.286	
Strut spanw. attachment pos.	η_s	0.792	

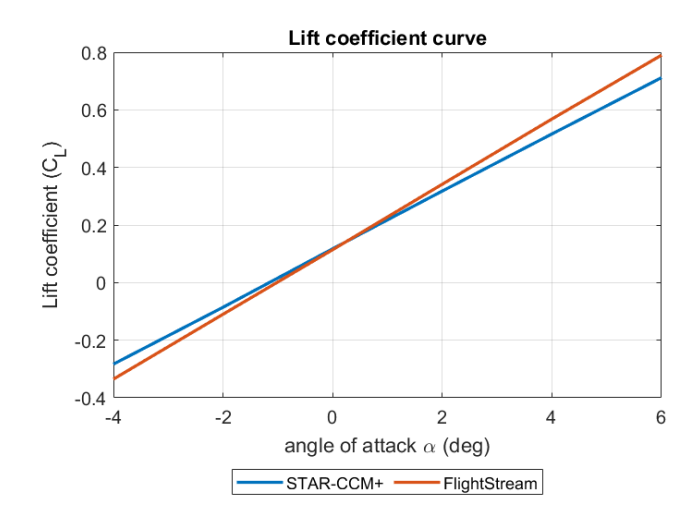


Figure 9 – Lift coefficient curve results comparison among STAR-CCM+ and FlightStream®.

where m_w represents the total mass of the wing configuration, m_{covers} denotes the wing box cover mass (including skins, stringers, and non-optimal mass penalties), $m_{webs+ribs}$ stands for the mass of the wing box spar webs and ribs, m_{sec} indicates the mass of the secondary wing structure, k_{ail} is the wingbox weight penalty factor for the wing box, necessary to meet aileron efficiency constraints. All the quantities defined in Equation (6) can be calculated using the equations (7), (8), (9), (10), (11), and (12).

$$m_{covers} = k_e \cdot C \cdot m_{TO}^{E_e} (W/S)^{E_{ws}} \mathcal{R}^{E_{\Lambda}} (\cos \Lambda)^{E_{\Lambda}} (t/c)^{E_{t/c}} V^{E_V} (1+\lambda)^{E_{\lambda}} n_z^{E_{nz}} (1-\eta)^{E_{\eta}}$$

$$\tag{7}$$

$$m_{webs+ribs} = k_e \cdot C \cdot m_{TO}^{E_e} (W/S)^{E_{ws}} \mathcal{R}^{E_{\Lambda}} (\cos \Lambda)^{E_{\Lambda}} (t/c)^{E_{t/c}} V^{E_V} (1+\lambda)^{E_{\lambda}} n_z^{E_{nz}} (1-\eta)^{E_{\eta}}$$
(8)

$$m_{strut} = k_e \cdot C \cdot m_{TO}^{E_e} (W/S)^{E_{ws}} \mathcal{R}^{E_{\Lambda}} (\cos \Lambda)^{E_{\Lambda}} (t/c)^{E_{t/c}} V^{E_V} (1+\lambda)^{E_{\lambda}} n_z^{E_{nz}} (1-\eta)^{E_{\eta}} P_{st}^{E_{pst}}$$
(9)

$$k_{ail} = \left(\frac{\eta_{ail}}{0.5}\right)^{-1.1}$$
, for conventional and SBW if $\eta_{ail} < 0.5$ (10)

$$k_{ail} = 1,$$
 for conventional and SBW if $\eta_{ail} >= 0.5$ (11)

$$\eta_{ail} = k_e \cdot C \cdot m_{TO}^{E_e} (W/S)^{E_{ws}} \mathcal{A} R^{E_{\Lambda}} (\cos \Lambda)^{E_{\Lambda}} (t/c)^{E_{t/c}} V^{E_V} (1+\lambda)^{E_{\lambda}} n_z^{E_{nz}} (1-\eta)^{E_{\eta}} P_{st2}^{E_{pst2}}$$
(12)

Here k_e represents the engine relief factor, W/S denotes the wing loading at takeoff condition, R

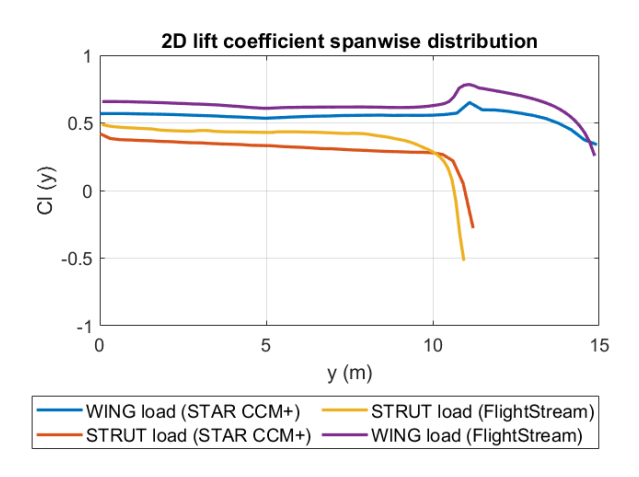


Figure 10 – Lift coefficient spanwise distribution comparison between STAR-CCM+ and FlightStream®, for $\alpha = 5 \ deg$, Re=12.5 mil.

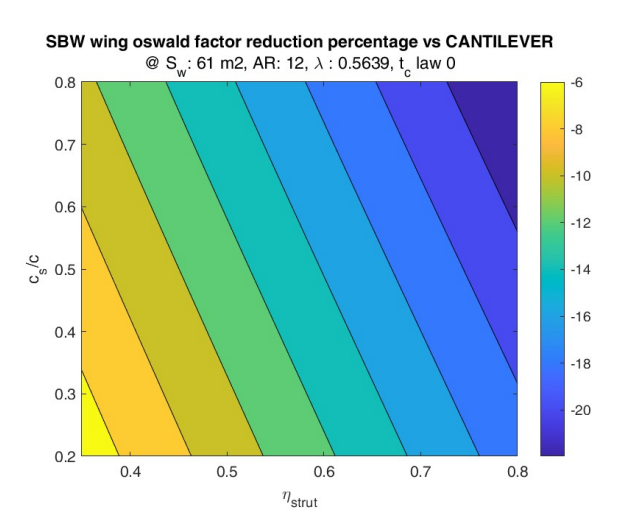


Figure 11 – Oswald's factor reduction model contour plot, for $S_w = 61 \text{ m}^2$, $\mathcal{R} = 12$, $\lambda = 0.5639$, t_c - set = Case-1.

stands for the wing aspect ratio, Λ indicates the wing sweep angle (c/2), t/c represents the airfoil thickness ratio, V denotes the maximum operating speed (EAS, m/s), λ signifies the wing taper ratio, n_z represents the design positive limit load factor, η denotes the strut position as a fraction of the wing span, p_{st} is the strut parameter (Equation (13)), η_{ail} represents the aileron efficiency at 67% of the maximum operating speed at sea level (defined as the ratio between the elastic and rigid rolling moment coefficient derivative due to aileron deflection), and p_{st2} is the second strut parameter (Equation (14)).

$$p_{st} = 1 - \eta^2 \sqrt{\frac{c_s/c}{R}} \tag{13}$$

$$p_{st2} = 2 - \frac{\eta}{\cos^2 \Lambda} \tag{14}$$

The coefficients C and exponents E for different materials (aluminum and composites) and wing configurations can be found in [24].

3. Regional turboprop with SBW application

3.1 Why the interest in evaluate a regional turboprop aircraft with SBW?

The aerodynamic model developed and the weight estimation method presented in the previous section are combined here to assess the impact of the SBW at the aircraft level, using the ATR72-600

regional turboprop aircraft as a reference platform. The choice of a regional turboprop aircraft as the test platform is based on the Bombardier market forecast for 2017-2036 [25], which indicates a total expected demand for 5750 regional turboprop and small single-aisle aircraft (80-150 seats) over the next 20 years. This demand arises because approximately 86% of the current fleet of these aircraft is expected to be retired by 2036. Considering these factors, it is crucial to investigate different technologies to produce a new regional aircraft that meets ACARE requirements and improves profitability by reducing Direct Operating Costs (DOC), such as through the use of new material technologies [26, 27]. The SBW solution appears to be a promising technology to address these challenges. Therefore, this paper focuses on understanding the impact of the strut, treated as a lifting body, on a SBW regional turboprop aircraft.

3.2 HEAD software

To assess the aerodynamic model at the aircraft level, the UNINA HEAD (Hybrid Electric Aircraft Designer) software was used. This software can handle the design of both conventional and hybrid-electric aircraft, including complex propulsive architectures such as Distributed Electric Propulsion (DEP). It ensures compliance with aeronautical regulations and design objectives [28]. The HEAD software consists of three modules:

- The *pre-design module*: Initializes the aircraft design based on Top-Level Aircraft Requirements (TLAR) using purely statistical methods [28].
- The *sizing module*: Estimates the required power and energy to perform a selected design mission and sizes the aircraft accordingly [29].
- The *analysis module*: Refines the aircraft design based on iterative simulation-based analysis of the reference mission [30]

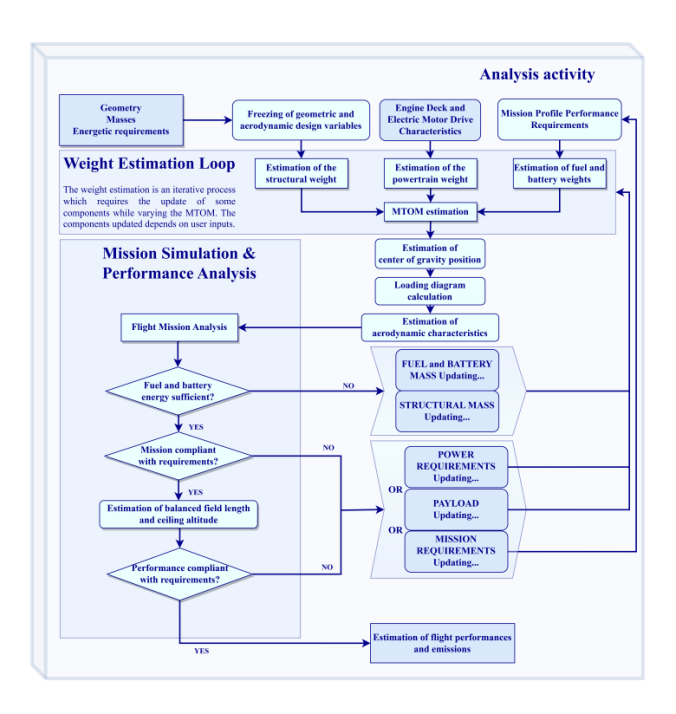


Figure 12 – Workflow of the HEAD software analysis model.

For this application, only the analysis module was used. The workflow for this process is depicted in the flowchart in Figure 12. This iterative process aims to estimate aircraft characteristics basing on the aircraft performance calculated in the previous design loop. Simulation-based analysis requires characterizing every step of the entire flight mission, considering factors such as Mach number, altitude, throttle setting, acceleration, and rate of climb. Depending on the flight segment, the algorithm executes three phases at each time step, as determined by the specific flight phase:

- Calculate the aerodynamic characteristics: Based on the flight conditions defined in the aircraft mission profile, aerodynamic characteristics are computed at the start of the flight segment simulation.
- Calculate the power distribution: At the prescribed airspeed and altitude, the power distribution along the propulsion system is determined.
- Estimate the new flight conditions: Based on aerodynamic and propulsive forces, new flight conditions are established.

To analyze the SBW version of the ATR72-600 aircraft, new methodologies were integrated into the HEAD software, specifically:

- Strut-braced wing weight estimation method, described in section 2.4
- New Drag estimation model for SBW concept 2.3

3.3 ATR72-600 HEAD model

To assess the impact of the SBW on the ATR72-600 aircraft, the HEAD model representative of the ATR72-600 must first be sized. The design assumptions for the ATR72 using the HEAD software are based on the information provided in the ATR72-600 brochure [31], as detailed in Table 5.

Table 5 – Design requirement assumed to size the ATR72 aircraft model using HEAD software [31]

Design Requirement	Value
Design Range	740 NM
Climb Speed	170 KCAS
Cruise Speed	270 KCAS
Diversion Range	100 NM
Holding Time	30 min
Fuel Reserve	5 %
Fuel Consumption in cruise @ 95 % MTOW - ISA - FL200	650 kg/h
Typical mission range	300 NM
Take-off field length @ MTOW - ISA - Sea Level	1315 m
Landing field length @ MLW - ISA - Sea Level	915 m

The HEAD analysis module was employed to size the HEAD aircraft model representative of the ATR72-600. In Table 6, the HEAD model results for the ATR72-600 are compared to the specifications declared by ATR to validate the software. The errors reported in the table demonstrate a sufficient level of fidelity in the results, providing confidence to proceed with estimating the impact of the SBW on the sized aircraft.

Table 6 – Comparison between ATR72-600 aircraft main parameters estimated using HEAD software with respect that reported on the brochure [31]

ATR72-600 HEAD model validation results.					
Parameter	Brochure	HEAD	Error (%)		
Max take-off mass	23 000 kg	23 264 kg	+ 1.14 %		
Max zero fuel mass	21 000 kg	21 365 kg	+1.73 %		
Operational empty mass	13600 kg	13965 kg	+2.68 %		
Max payload	7400 kg	7400 kg	/		
Take-off field length	1315 m	1308 m	- 0.53 %		
Landing field length	915 m	950 m	+ 3.8 %		
Block fuel for 300 NM	869 kg	857 kg	- 1.38 %		
Block time for 300 NM	01:24 h	01:14 h	- 11 %		
CO_2 emissions for $300\mathrm{NM}$	2.75 ton	2.7 ton	-1.8 %		

3.4 ATR72-600 SBW version

This section evaluates the potential benefits of the new wing technology for the ATR72-600 regional turboprop aircraft in terms of fuel savings and pollution reduction. Through the use of the HEAD software has been possible to assesses the effect of this new wing architecture using the developed aerodynamic surrogate model sizing different versions of the ATR72-600 SBW. This analysis employed a full factorial Design of Experiments (DOE) approach, using S_w , AR, and c_s/c as design variables. Table 7 lists the design variables, their boundaries, and the number of levels used in this investigation, resulting in a total of 125 cases. To comprehend the actual impact of the developed surrogate model, the HEAD analysis model was used to design the aircraft both with and without considering the change in the Oswald factor caused by the wing-strut interference model.

Table 7 – Geometric design variables used to perform the full factorial DOE ATR72-600 investigation.

Full factorial design variables					
Variable Description Min. value Max. value					
S_W	wing area	50 m ²	$70\mathrm{m}^2$	5	
R	wing aspect ratio	10	17	5	
c_s/c	strut chord ratio	0.2	0.4	5	
η_s	strut attachment semi-spanwise position	0.66	0.66	1	
t_c	wing thickness ratio sets	Case-1	Case-1	1	
λ	wing taper ratio	0.5639	0.5639	1	

Table 8 illustrates the impact of wing surface and aspect ratio on MTOW for the SBW configuration, considering variable c_s/c with a fixed value of η_s set at 66% of the semispan. The choice of 66% of the semispan is based on key findings by Zhang et al. [32], which showed that to reduce the structural weight of the wing, the ideal strut position should be between 60% and 70% of the wingspan.

As the strut chord ratio increases, there is a reduction in MTOW for both analysis cases. The main difference between the results obtained using the two drag models lies in the shape of the contour lines and a slight reduction in MTOW when not considering the reduction in the Oswald factor, resulting in lower required propulsive power at takeoff. When considering the increase in drag caused by the developed aerodynamic surrogate model, there is a slight rise in MTOW. The contour plots also show a specific region on the wing surface (around $60\,\mathrm{m}^2$) where MTOW is minimized with the highest range in wing aspect ratio. The maximum AR at which it is possible to maintain a low MTOW value increases with an increase in the strut chord ratio. This phenomenon is attributed to the beneficial strut effect on wing weight. A greater chord allows the strut to absorb more load, leading to a higher reduction in the wing root bending moment. This reduction lowers the necessary wing stiffness and, consequently, reduces the overall wing weight.

Table 9 illustrates the impact of wing surface area and aspect ratio on the block fuel percentage variation for the SBW configuration, considering variable c_s/c with a fixed value of η_s set at 66% of the semi-span. These contour plots identify an optimal wing surface area where fuel consumption is minimized, approximately between $60\,\mathrm{m}^2$ and $65\,\mathrm{m}^2$. By comparing contour plots with the same strut chord ratio, we observe higher block fuel savings when not considering the developed aerodynamic model. This is because lower drag requires less fuel for the assigned mission. Comparing the results with a constant strut chord ratio value shows that maximum fuel savings are achieved with high aspect ratio values. With a low aspect ratio, a larger strut chord (i) increases the parasite drag coefficient, (ii) significantly impacts wing loading, resulting in a high $k_{\rm red}$ value, and (iii) the reduction in wing weight at low AR values for a SBW is not sufficient to counteract the aerodynamic drawbacks. Without the aerodynamic surrogate model, results are quite similar, but even with a not very high aspect ratio, there is significant fuel saving.

From the block fuel reduction contour plots, a region with maximum fuel savings can be identified. The surface area corresponding to maximum fuel savings is approximately $60\,\mathrm{m}^2$, coinciding with the surface area where the minimum MTOW value was registered. This surface value can be explained by

Table 8 – Max take off weight (MTOW) [tons] contour plots for the sized ATR72-600 SBW version with and without using the surrogate aerodynamic model to estimate the reduction in the Oswald efficiency factor.

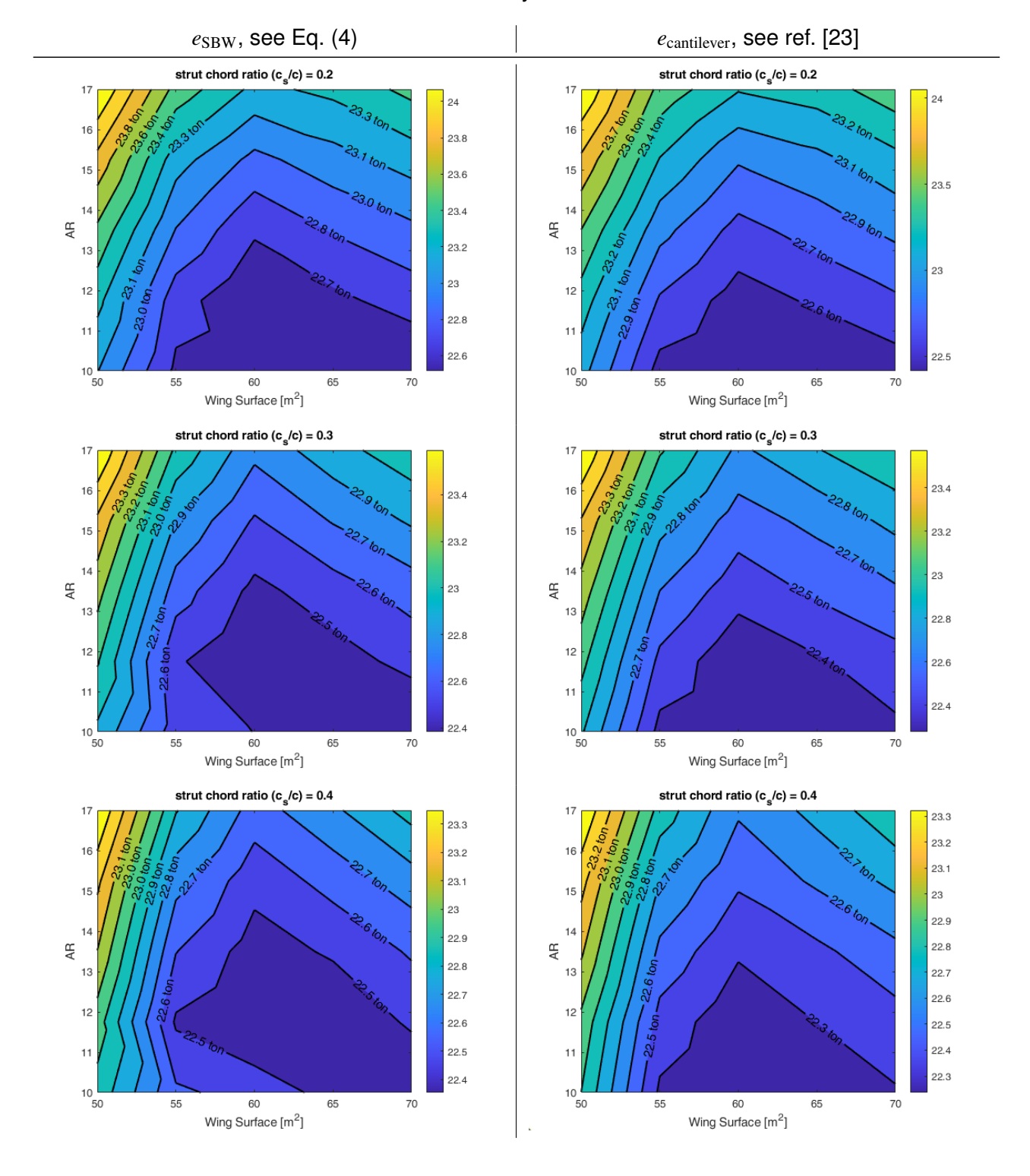
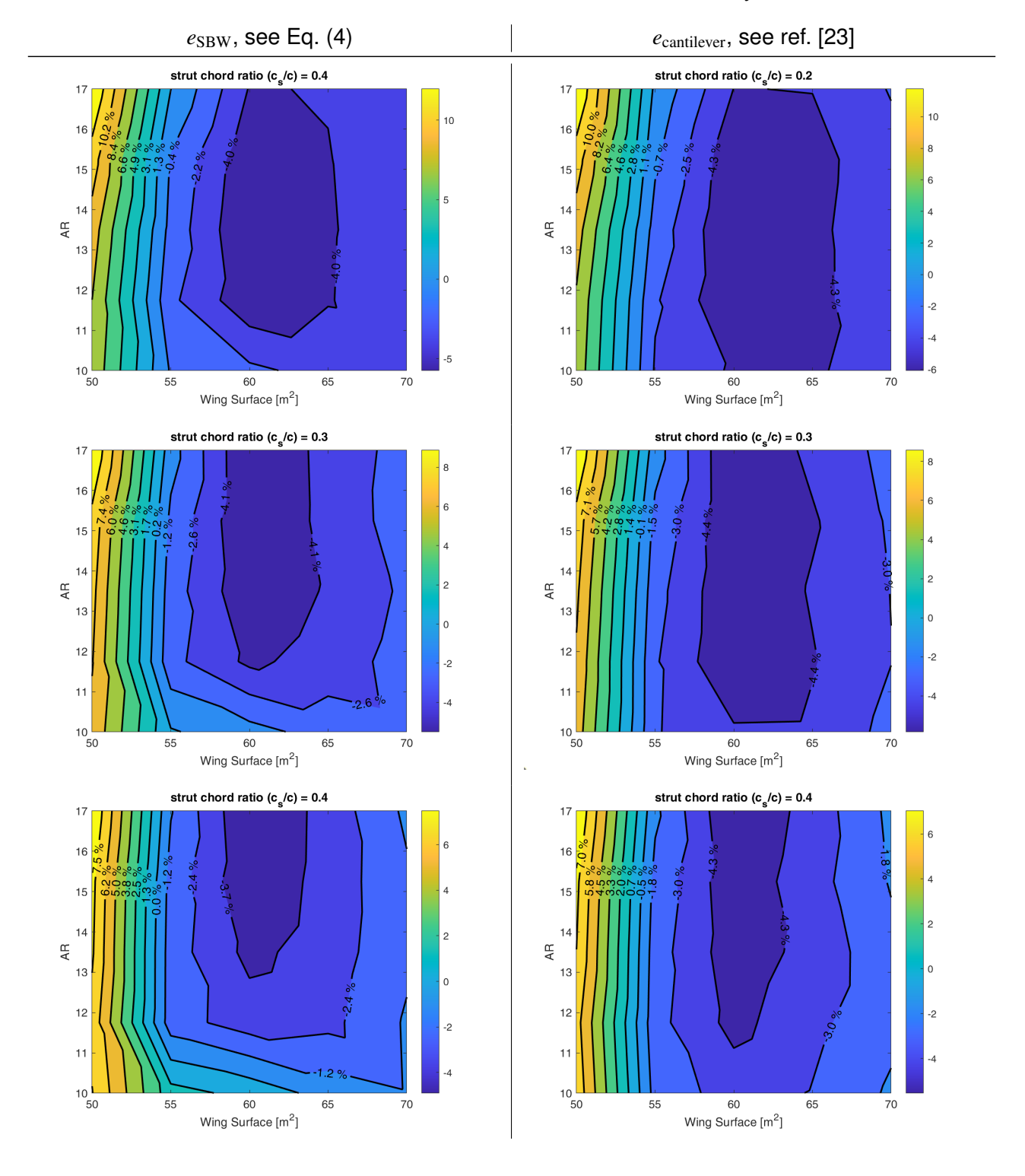
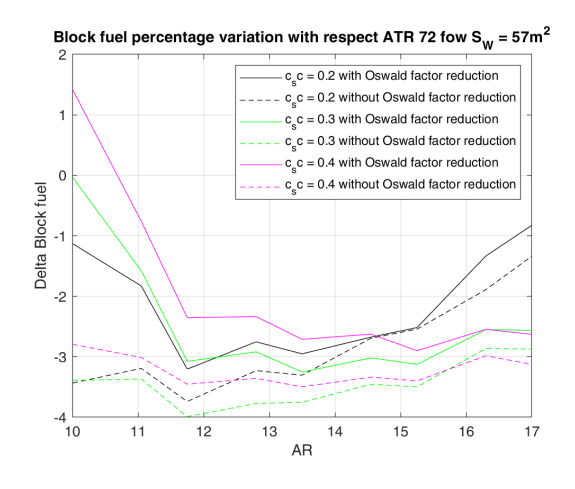


Table 9 – Percentage change in block fuel (300 NM typical mission) with respect to the baseline aircraft, for the sized ATR72-600 SBW version with and without using the surrogate aerodynamic model to estimate the reduction in the Oswald efficiency factor.



the fact that a smaller wing surface area results in increased drag due to a larger strut chord, reducing the already limited takeoff capabilities associated with a small wing area configuration. An increase in wing surface helps improve take-off capability, but this benefit is valid only up to a certain value. For a wing surface area exceeding $65\,\mathrm{m}^2$, the advantage gained in take-off capability is counteracted by increased aircraft drag caused by the larger wetted area, leading to reduced fuel saving. Based on these considerations, the effect of fuel percentage variation near the optimal wing surface value was analyzed in detail. Four different wing surface areas were chosen for analysis: $S_w = 57\,\mathrm{m}^2$, $S_w = 60\,\mathrm{m}^2$, $S_w = 63\,\mathrm{m}^2$, and $S_w = 65\,\mathrm{m}^2$. These values are plotted in Figures 13, 14, 15, and 15, respectively.

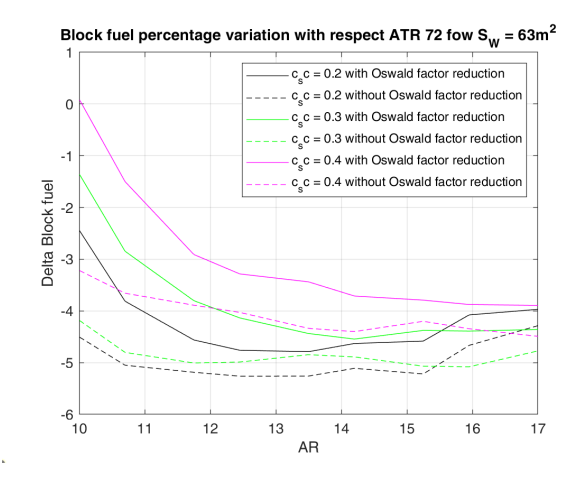


Block fuel percentage variation with respect ATR 72 fow S_w = 60m²

c_s c = 0.2 with Oswald factor reduction
c_s c = 0.3 with Oswald factor reduction
c_s c = 0.3 without Oswald factor reduction
c_s c = 0.4 with Oswald factor reduction
c_s c = 0.4 with Oswald factor reduction
c_s c = 0.4 without Oswald factor reduction
c_s c = 0.4 without Oswald factor reduction
AR

Figure 13 – Block fuel variation percentage w.r.t. baseline vs AR, for different strut chord ratio values with and without the use of the aerodynamic surrogate model($S_w = 57 \text{ m}^2$).

Figure 14 – Block fuel variation percentage w.r.t. baseline vs AR, for different strut chord ratio values with and without the use of the aerodynamic surrogate model($S_w = 60 \text{ m}^2$).



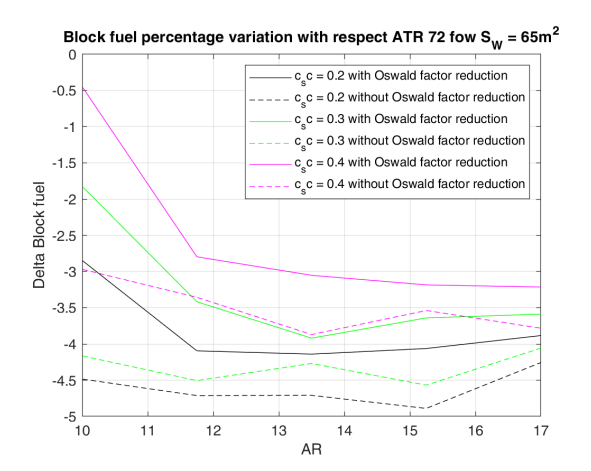


Figure 15 – Block fuel variation percentage w.r.t. baseline vs AR, for different strut chord ratio values with and without the use of the aerodynamic surrogate model($S_w = 63 \text{ m}^2$).

Figure 16 – Block fuel variation percentage w.r.t. baseline vs AR, for different strut chord ratio values with and without the use of the aerodynamic surrogate model($S_w = 65 \text{ m}^2$).

In these figures, the impact of the wing aspect ratio on block fuel for various strut chord ratio values with and without utilizing the Oswald factor variation surrogate model is observed, while keeping the wing surface values constant. As previously discussed, the optimal wing surface for this analysis is $60\,\mathrm{m}^2$, resulting in a fuel saving of about -5.75% to -6% depending on whether the developed aerodynamic surrogate model is considered.

Focusing on Fig. 14 for a fixed strut chord ratio value, the chart can be subdivided into three different regions: *low AR region*, *mid AR region*, and *high AR region*, based on the AR value at which maximum fuel saving exists.

Let's discuss the black curves where $c_s/c = 0.2$.

In the *low AR region* (10 < AR < 12), a high difference is observed between the two solutions. The utilization of the surrogate model leads to a reduction in fuel savings by approximately 50%. This difference occurs because, at low AR values, wing loading is significantly affected by the interference effect of the wing strut. This increase in drag is not yet counteracted by the beneficial effect of weight reduction resulting from the SBW configuration. As the strut chord ratio increases, the difference in fuel savings between the two results increases.

In the $mid\ AR\ region\ (12 \le AR < 15)$, the difference between the two results decreases, indicating a consistent trend. The reduction in error between the two solutions can be understood by considering the weight benefit from the strut and the aerodynamic advantage from an increased AR, which helps to bridge the gap between the two solutions. The gap exists because of the additional drag caused by the induced drag model. AR = 13.5 is the optimal AR point, beyond which increasing AR does not produce the expected aerodynamic benefit for fuel savings. As the AR of the wing increases, the strut becomes wider, increasing the wetted area and consequently the drag. Additionally, the weight benefit achieved when increasing the aspect ratio using a low strut chord ratio is not as significant as with a higher strut chord ratio.

In the *high AR region* ($AR \ge 15$), the two curves decrease because the aerodynamic effect produced by the surrogate model diminishes.

The same behavior discussed for $c_s/c = 0.2$ is applicable when increasing the strut chord ratio. Given that the design space does not clarify if this trend exists for other solutions, the design space was extended only for this wing surface value, and the results are reported in Figure 17.

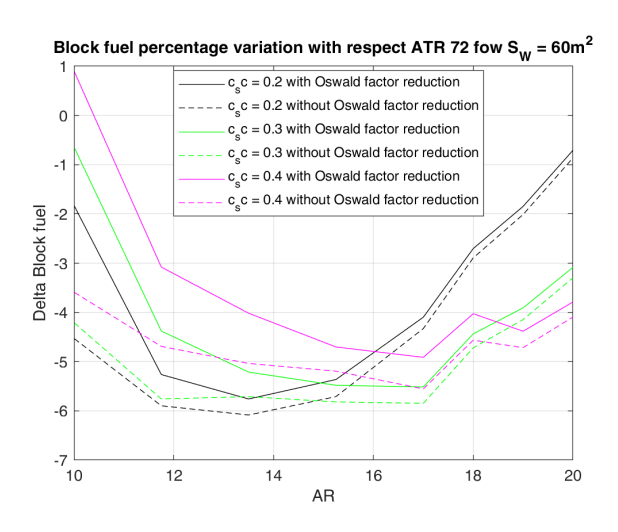


Figure 17 – Block fuel variation percentage w.r.t. baseline vs AR, for different strut chord ratio values with and without the use of the aerodynamic surrogate model($S_w = 60 \,\mathrm{m}^2$), design space extended.

From the figure, it can be seen that the same discussion valid for $c_s/c=0.2$ curves can be applied to the solutions with higher strut chord ratios. In particular, it can be observed that the optimal strut chord ratio value is $c_s/c=0.3$, where a block fuel saving of 5.51% (solid green line) and 5.9% (solid dashed line) at AR = 17 can be estimated. Additionally, as the strut chord ratio increases, the gap between the two solutions at the minimum point also increases. This effect can be attributed to the additional drag caused by the wing-strut interference, which escalates with the increase in strut chord ratio. The solution with the highest strut chord ratio leads to the lowest fuel savings due to the greater increase in drag from using a larger strut chord. For this aircraft and mission, the increase in drag outweighs the weight-saving benefits.

4. Conclusions and future work

This study identifies a SBW configuration that, when applied to the baseline ATR72-600 aircraft, reduces block fuel consumption and, consequently, CO₂ emissions. The results indicate that utilizing the developed induced drag model decreases fuel savings by approximately 4.1% for the lowest strut chord ratio configuration and about 6.6% for the configuration with the optimal strut chord ratio $(c_s/c = 0.3)$. The optimal configuration is deemed the best solution due to its significant fuel savings when the aspect ratio is large. Thus, the ATR72-600 SBW configuration with the most substantial fuel consumption reduction is $S_w = 60 \,\mathrm{m}^2$, AR = 17, $c_s/c = 0.3$, $\lambda = 0.5639$, t_c -set = Case-1, $\eta_s = 0.66$. While the variation in block fuel due to the application of the developed aerodynamic model seems minor, its actual impact can be assessed by comparing a year of flights for the baseline aircraft versus the new ATR72-600 SBW version with and without using the surrogate aerodynamic drag model. The results, shown in Table 10, are based on a typical mission of 300 NM, allowing for six flights per day over 358 days a year, accounting for seven days of maintenance. Table 11 presents the differences between the three aircraft configurations discussed. The SBW version, sized using the induced drag aerodynamic model, saves up to 101 tons of fuel annually, while not considering the model saves an additional 9 tons. The third column highlights the difference between the two SBW solutions, indicating that neglecting the wing-strut interaction effect overestimates annual fuel savings by about 9 tons.

In conclusion, the introduction of induced drag modeling for regional turboprop aircraft enhances the accuracy of SBW configurations in the preliminary design phases. Many researchers have focused on sizing aircraft without considering the strut as a lifting body, neglecting the wing-strut interaction effect, which impacts the wing's aerodynamic loading and, consequently, the aircraft's induced drag. The use of this surrogate aerodynamic model provides more reliable results. It is important to note that the difference compared to the non-lifting strut solution increases as the strut chord ratio increases, while it decreases as the wing aspect ratio increases. This aerodynamic model could be further improved by increasing the accuracy of the aerodynamic solver or by designing a better shape for the primary wing strut with a rounded wing-strut junction, which would decrease aerodynamic interaction effects.

Table 10 – Annual flight results for the baseline aircraft and the designed ATR72-600 SBW versions

Annual flight consumption comparison					
$egin{array}{ c c c c c c c c c c c c c c c c c c c$					
Block fuel per mission (kg / Flight)	857	806	810		
Block fuel per day (kg / Day)	5142	4836	4860		
Block fuel per year (ton / Year)	1841	1731	1740		
CO ₂ emitted per year (ton / Year)	5818	5471	5498		

Table 11 – ATR72-600 SBW versions result delta comparison w.r.t. baseline aircraft.

ATR72-600 SBW comparison					
$ e_{ m cantilever}$ vs. baseline $ e_{ m SBW}$ vs. baseline $ e_{ m SBW}$ vs. $e_{ m cantilever}$					
Block fuel per mission (kg / Flight)	-51	-47	4		
Block fuel per day (kg / Day)	-306	-282	24		
Block fuel per year (ton / Year)	-110	-101	9		
CO ₂ emitted per year (ton / Year)	-347	-320	27		

5. Contact Author Email Address

To contact mailto: giuseppe.grazioso@unina.it

6. Copyright Statement

The authors confirm that they, and/or their company or organization, hold copyright on all of the original material included in this paper. The authors also confirm that they have obtained permission, from the copyright holder of any third party material included in this paper, to publish it as part of their paper. The authors confirm that they give permission, or have obtained permission from the copyright holder of this paper, for the publication and distribution of this paper as part of the ICAS proceedings or as individual off-prints from the proceedings.

References

- [1] Scafaer M. Forecast of Air Traffic's CO2 and NOx Emissions until 2030. 17th Air Transport Research Society (ATRS) World Conference, Bergamo 2013.
- [2] European Commission Directorate-General for Mobility and Transport, Directorate-General for Research and Innovation, *Flightpath 2050 Europe's vision for aviation Maintaining global leadership and serving society's needs*, Publications Office, 2011.
- [3] Advisory Council for Aviation Research and Innovation in Europe (ACARE). Fly the Green Deal, 2022. https://www.acare4europe.org/wp-content/uploads/2022/06/20220815_Fly-the-green-deal_LR-1.pdf.
- [4] Corcione S., Mandorino M., Cusati V. "Beyond conventional: An integrated aerostructural optimization approach for innovative tailplane configurations". *Aerospace Science and Technology* 2024 https://doi.org/10.1016/j.ast.2024.109242
- [5] Corcione S., Cusati V., Memmolo V., Nicolosi F., Nicolosi F., "Impact at aircraft level of elastic efficiency of a forward-swept tailplane", *Aerospace Science and Technology* 2023
- [6] Cusati V., Corcione S., Nicolosi F., Zhang Q., "Improvement of Take-Off performance for an Electric Commuter Aircraft Due to Distributed Electric Propulsion", *Aerospace 2023*, 10,276. https://doi.org/10.3390/aerospace10030276
- [7] Tianlong L., Pecora R., Ciliberti D., Xia W., Hu S., "Aerodynamic optimization of an adaptive flap for next-generation green aircraft", *Chinese Journal of Aeronautics* 2024. 10.1016/j.cja.2023.10.010
- [8] Abu Salem K., Palaia G., Quarta A.A. "Review of hybrid-electric aircraft technologies and designs: Critical analysis and novel solutions". *Progress in Aerospace Science*, 2023, vol. 141. https://doi.org/10.3390/aerospace10050459
- [9] Abu Salem K., Palaia G., Quarta A.A., "Impact of Figures of Merit Selection on Hybrid-Electric Regional Aircraft Design and Performance Analysis", Energies, 2023, vol.16 https://doi.org/10.3390/en16237881
- [10] Palaia G., Abu Salem K., Quarta A.A. "Parametric Analysis for Hybrid-Electric Regional Aircraft Conceptual Design and Development". Applied Sciences, 2023, vol 13. https://doi.org/10.3390/app131911113
- [11] Abu Salem K., Palaia G., Bravo-Mosquera Pedro D., Quarta A.A., "A Review of Novel and Non-Conventional Propulsion Integrations for Next-Generation Aircraft", *Designs*, 2024, vol. 8 https://doi.org/10.3390/designs8020020
- [12] Ma Y., Yan J., Elham A. "Initial weight estimation of twin-fuselage configuration in aircraft conceptual design". *Proceedings of the Institution of Mechanical Engineers, Part G: Journal of Aerospace Engineering* 2023; 237(1): 130-140 doi:10.1177/09544100221095370.
- [13] Bradley M. K., Droney C. K., and Allen T. J., "Subsonic Ultra Green Aircraft Research Phase II: Volume I Truss Braced Wing Design Exploration," *NASA CR-2015-218704/Volume I*, 2015.
- [14] Research in Flight company, FLIGHTSTREAM®, 2020, https://researchinflight.com/products.html.
- [15] Burkhalter J.E., Ahuja V., Hartfield R., "Robust prediction of high lift using surface vorticity" *NASA SBIR NNX17XL12C PhaseII final report* 2017.
- [16] Ahuja V., Hartfield R.J., "Aerodynamic Loads over Arbitrary Bodies by Method of Integrated Circulation", *Journal of Aircraft* Vol. 53, No. 6(2016), pp.1719-1730.
- [17] SmartUp Engineering S.r.I., JPAD Modeller, https://www.smartup-engineering.com/pricing
- [18] Trifari V.,Ruocco M.,Cusati V.,Nicolosi F. and De Marco A., "Multidisciplinary analysis and optimization Java tool for aircraft design". *ICAS 31st Congress of the International Council of the Aeronautical Sciences* Belo Horizonte, Brazil,2018, ISBN: 9783932182884.

Strut-Braced Wing Induced Drag Modeling for Regional Turboprop Aircraft Design

- [19] Trifari, V., Ruocco, M., Cusati, V., Nicolosi, F., and De Marco, A. "Java Framework for Parametric Aircraft Design Ground Performance". *Aircraft engineering and Aerospace Technology (AEAT)*, Vol. 89, No. 4, 2017, pp. 599–608, doi: http://dx.doi.org/10.1108/AEAT-11-2016-0209.
- [20] Nicolosi F., De Marco V., Attanasio L., and Della Vecchia P., "Development of a Java-based framework for aircraft preliminary design and optimization," *AIAA Journal of Aerospace Information Systems*, Vol. 13, No. 16, 2016, pp. 234-242, doi: https://doi.org/10.2514/1.1010404.
- [21] Trifari V., De Marco A., Di Stasio M., Ruocco M., Nicolosi F., Grazioso G., Ahuja V., Hartfield R.J., "An aircraft design workflow using the automatic knowledge-based modelling tool JPAD Modeller" *AIAA AVI-ATION Forum* July 2022, Chicago, https://doi.org/10.2514/6.2022-3737
- [22] Simcenter STAR-CCM+ CFD software https://plm.sw.siemens.com/it-IT/simcenter/fluids-thermal-simulation/star-ccm/.
- [23] Nita M. and Scholz D., "Estimating the Oswald Factor from basic aircraft geometrical parameters", 2012.
- [24] G.P. Chiozzotto, "Initial weight estimate of advanced transport aircraft concept considering aeroelastic effects", *AIAA Paper*, Jan. 2017, https://doi.org/10.2514/6.2017-0009
- [25] Market forecast, 2017-2036. Bombardier 2017. https://bombardier.com/en/media/news/bombardier-commercial-aircrafts-new-20-year-2017-2036-market-forecast-shows-strong
- [26] Cusati V., Corcione S., Memmolo V. "Potential Benefit of Structural Health Monitoring System on Civil Jet Aircraft". Sensors 2022; 22(19):7316 https://doi.org/10.3390/s22197316
- [27] Cusati V., Corcione S., Memmolo V. "Impact of Structural Health Monitoring on Aircraft Operating Costs by Multidisciplinary Analysis". *Sensors* 2021; 21(20):6938 https://doi.org/10.3390/s21206938
- [28] Orefice F., Della Vecchia P., Ciliberti D. and Nicolosi F., "Aircraft Conceptual Design Including Powertrain System Architecture and Distributed Propulsion," 2019 AIAA/IEEE Electric Aircraft Technologies Symposium (EATS), Indianapolis, IN, USA, 2019, pp. 1-20, doi: 10.2514/6.2019-4465.
- [29] Marciello V., Orefice F., Nicolosi F., Ciliberti D., "Design of hybrid-electric aircraft with falut-tolerans considerations". *Chinese Journal of Aeronautics* June 2022, 36, 160-178.
- [30] Orefice F., Nicolosi F., Corcione S., Della Vecchia P., "Hybridization and Mission Analysis of a regional turboprop", *AIAA AVIATION FORUM* August 2021.
- [31] ATR72-600 brochure https://www.atr-aircraft.com/wp-content/uploads/2022/06/ATR_Fiche72-600-3.pdf.
- [32] Zhang X., Zhang S., Wang J., Zhou B., "Effect of primary parameters on structure weight of civil aircraft with strut-braced wing", *ACTA AERONAUTICAET ASTRONAUTICA SINICA* Vol.40, 2019. DOI: 10.7527/S1000-6893.2018.22359